Characterizing Tyrosine Ring Flips in Proteins by ^{19}F NMR

Meng Lu[1,2], Guohua Xu[1,2,*], Qiong Wu[1,2], Xiaoli Liu[1,2], Mingjuan Yang[1,2], Ling Jiang[1,2], Minghui Yang[1,2], Maili Liu[1,2], Conggang Li[1,2,*]

[1] Key Laboratory of Magnetic Resonance in Biological Systems, State Key Laboratory of Magnetic Resonance and Atomic and Molecular Physics, National Center for Magnetic Resonance in Wuhan, Wuhan National Laboratory for Optoelectronics, Wuhan Institute of Physics and Mathematics, Innovation Academy for Precision Measurement Science and Technology, Chinese Academy of Sciences, Wuhan, 430071, P. R. China.

[2] University of Chinese Academy of Sciences, Beijing, 100049, P.R. China.

* To whom correspondence should be addressed. Email: conggangli@wipm.ac.cn (Conggang Li) guohua_xu@apm.ac.cn (Guohua Xu)

ABSTRACT

Aromatic ring flip dynamics are essential for elucidating the catalytic mechanism of enzyme, protein binding, and the "breathing" motions of proteins. NMR is the primary method for measuring aromatic ring flip rates in proteins at the residue level, but it typically requires extreme conditions such as high pressure or low temperature to slow down the ring flips to a detectable rate on the NMR time scale. Consequently, ring flip rates have only been measured for a limited number of proteins due to the lack of simple method under mild conditions. Here we report a novel ^{19}F NMR method utilizing 2,6-difluoro-tyrosine (2,6-F_2Y) substitution to measure the ring flip rate of tyrosine residues *in vitro* and in living cells. We validated the effectiveness of method on three proteins, the B1 domain of protein G (GB1), ubiquitin (UBQ) and histidine-containing phosphocarrier protein (HPr). The results demonstrated that this ^{19}F NMR approach can quantify the ring flip on timescales from microseconds to seconds under mild experimental conditions. For the first time, we measured the tyrosine ring flip dynamics of HPr in three types of living cells: *E. coli*, A2780 cells and *X. laevis* oocytes. Our findings reveal that tyrosine ring flip dynamics are remarkably affected by cellular environment and are cell-type dependent. The strong interactions and the low activation enthalpy are associated with fast ring flipping. Our study provides a simple, convenient and efficient method for characterizing tyrosine ring flip in proteins both *in vitro* and in cells, and it also opens a new avenue for measuring the ring flip rates in proteins in complex biological environments.

TOC

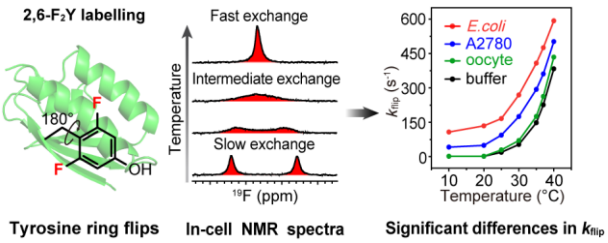

INTRODUCTION

Aromatic residues have several prominent functions. They are found at the protein interface, facilitating protein binding and enzyme catalysis,[1-3] and in the hydrophobic core of folded proteins, where they stabilize protein structure through π-π, CH-π, and cation-π interactions.[4-7] The aromatic rings of phenylalanine (Phe) and tyrosine (Tyr) can undergo ring flips, i.e., 180 ° rotations around the C_β-C_γ-C_ζ axis (Figure 1A), despite their tight packing in the hydrophobic core of the protein.[8-15] Studying these ring flip dynamics, e.g., the ring flip rate (k_{flip}), provides insights into enzyme catalytic mechanisms, protein binding, and the "breathing" motions of proteins, revealing the internal dynamic properties.[2, 16-18]

Nuclear magnetic resonance (NMR) spectroscopy, with its atomic resolution and non-invasive nature, has been used to characterize aromatic ring flip dynamics since the pioneering observations in the 1970s.[19-22] When using NMR methods to accurately measure aromatic ring flip rates, the chemical shift difference $\Delta\omega$ and the exchange rate k_{ex} ($k_{flip} = k_{ex}/2$) between the two symmetry-related nuclei of the aromatic ring directly affect the appearance of the spectrum.[18] In the slow exchange regime ($k_{ex} < \Delta\omega$) on the NMR time scale, the two separate peaks can be observed for the two symmetry-related nuclei of the aromatic ring. The line widths of the two peaks depend on k_{ex} in relation to $\Delta\omega$. In the intermediate regime ($k_{ex} \approx \Delta\omega$), the line width broadens up to disappear. In the fast exchange regime ($k_{ex} > \Delta\omega$), a single peak is observed at the midpoint of the two separate peaks observed under slow exchange conditions. NMR methods such as line shape analysis or exchange spectra to measure ring flip rate, require the observation of two separate signals in the slow exchange regime.[2, 9-12, 23-24] However, at normal temperature and pressure (NPT), the aromatic side chains usually flip with a $k_{flip} > 10^3$ s^{-1}, and exhibits a fast exchange in ^{1}H and ^{13}C NMR spectra due to $k_{ex} > \Delta\omega$. Thus, some extreme conditions such as high pressure and/or low temperature (below 0 °C) are required to slow down the ring flip rate to a slow exchange regime on the NMR time scale.[10, 13, 25] Although it is not necessary to obtain the $\Delta\omega$ value for NMR methods such as CPMG and $R_{1\rho}$ relaxation dispersion experiments to measure the flip rate.[13-15, 26-29] The signal assignments for aromatic ring protons are challenging for proteins and costly site-selective ^{13}C isotope labelling of aromatic side chains are required.[2, 29] Limited by these demanding conditions, to date, the ring flip rates have only been measured for a limited number of small proteins, such as BPTI, Cyt c, Bcx, HPr, FKBP12 and GB1. Additionally, these developed methods, which require extreme conditions, are difficult to apply to the study of ring flip in living cells, where the crowded and complex

environments cause strong background interference and signal broadening, making the data analysis complicated.[30] Therefore, a simple and effective method to characterize the ring flip dynamics *in vitro* and in cells is needed.

^{19}F has favorable NMR properties such as a spin-1/2 nucleus, 100% abundance, high sensitivity (83% of ^{1}H), and near-absence in nature biological systems. ^{19}F has been widely used as a sensitive probe in the NMR study of proteins *in vitro* and in cells.[31-44] Compared to ^{13}C and ^{1}H nuclei, fluorine resonances are exquisitely sensitive to subtle changes in their environments, owing to an anisotropic distribution of electrons in the fluorine 2p orbitals, their chemical shift range is over 400 ppm for organ fluorine compounds. This means that if fluorinating aromatic rings in proteins, the much larger chemical shift difference ($\Delta\omega$) compared to ^{1}H/^{13}C would be obtained, the ring flip process, which shows a fast exchange in NMR spectra for the ^{1}H/^{13}C nucleus ($k_{ex} > \Delta\omega$), may manifest as a slow exchange for the ^{19}F nucleus. Additionally, the introduction of the ^{19}F into proteins may also enhance the hydrophobic interaction and thus slow down the ring flip rate, due to the increased hydrophobicity of fluorocarbons relative to hydrocarbons. The combined results may lead to the direct observation of the two separate slow-exchange ^{19}F signals under mild conditions. To validate this hypothesis, here we develop a fluorine-substituted tyrosine probe sensitive to the ring flips process and investigate the ring flip rates of tyrosine residues of various proteins. We demonstrate that the ^{19}F NMR method is a simple and universal to investigate their ring flip rates in various environments including dilute solution, crowded environments and living cells, which open up an avenue for our understanding of ring flip events of proteins in complex biological environments.

MATERIALS AND METHODS

Enzymatic synthesis of F_nYs

2-fluorophenol, 3-fluorophenol, 2,3-difluorophenol, 2,5-difluorophenol, 2,6-difluorophenol, 3,5-difluorophenol, pyridoxal-5′-phosphate (PLP), Celite® 545 were purchased from Aladdin (Shanghai, China). $^{15}NH_4Cl$ was purchased from Cambridge Isotope Laboratories, Inc. (Andover, USA). Sodium pyruvate, ethyl acetate were purchased from Sinopharm Chemical Reagent Co., Ltd. (Shanghai, China). All reagents were used without further purification.

The enzyme tyrosine phenol lyase (TPL) was obtained as described with slight modifications.[45] Its encoding gene from C. *freundii* (NCBI accession No. L10821.1) was synthesized by Sangon

Biotechnology Co., Ltd. (Shanghai, China), and cloned into a pET-28a vector with restriction sites BamHI/HhoI under T7 promoter. TPL purification was performed using HisTrap Ni-NTA affinity column with buffer A (50 mM KH_2PO_4-K_2HPO_4, 500 mM NaCl, 10 mM imidazole, pH 7.5) and buffer B (50 mM KH_2PO_4-K_2HPO_4, 500 mM NaCl, 500 mM imidazole, pH 7.5) at 4 ℃. The purified TPL was buffer exchanged to 20 mM KH_2PO_4-K_2HPO_4, pH 7,5, and stored at -80 ℃.

Fluorotyrosines (F_nYs) were synthesized as described.[46] The final products were identified by ^{19}F NMR and ESI-MS. The F_nY yield (Y_{F_nY}) could be calculated as follows:

$$Y_{F_nY} = \frac{Y_{F_nY,T}\alpha I_{F_nY,2}V_2}{I_{F_nY,1}V_1} \qquad \text{eq 1}$$

where $I_{F_nY,1}$ and $I_{F_nY,2}$ are the ^{19}F integral intensities of F_nY, using 4-F phenylalanine as a reference, in reaction solution and final product solution, respectively. V_1 and V_2 are the volume of reaction solution and final product solution, respectively. α is the reaction conversion rate, and $Y_{F_nY,T}$ is the theoretical yield of F_nY.

Protein expression and purification

The plasmids containing genes for GB1 and UBQ were home-owned. The encoding gene from *Staphylococcus carnosus* for HPr (UniProtKB P23534) was synthesized and cloned into a pET-28a vector with restriction sites NcoI/XhoI under T7 promoter by Sangon Biotechnology Co., Ltd. (Shanghai, China). Mutations were introduced by site-directed mutagenesis. The needful primers were synthesized by Sangon Biotechnology Co., Ltd. (Shanghai, China)

The plasmids containing corresponding protein genes were transformed into *E. coli* BL21(DE3) competent cells, respectively. Plasmid-containing cells for GB1 and its mutants (Y3F, Y33F, Y45F) and UBQ were selected with 100 μg/mL of ampicillin, and ^{19}F-labelled protein expression and purification were performed as described.[47-48] Plasmid-containing cells for HPr and its mutants (Y6F, Y37F, Y64F) were selected with 50 μg/mL of kanamycin and purified as described with slight modifications.[49] Briefly, the cell pellet was resuspended in 50 ml buffer A (20 mM NaPB, pH 7.0), containing 500 μL protease inhibitor cocktail (100x), 1mg DNase. The suspension was passed several times through ATS high pressure homogenizer at 900 bar, and cell debris was removed by centrifugation at 20,000 rpm for 30 min at 4 ℃. The supernatant was applied to a DEAE Fast Flow column (GE Healthcare) with buffer A and buffer B (20 mM NaPB, 1 M NaCl, pH 7.0), followed by size exclusion chromatography with buffer C (20 mM Tris, 150 M NaCl, pH 7.5). All purified proteins were lyophilized and stored at -80 ℃ after

desalting.

NMR Experiments

For *in vitro* NMR, the measurements involving temperature-variable below 0 ℃ were performed using eight 1.1 mm o.d. glass capillary tubes within a regular 5 mm NMR tube.[25, 50] Samples were centrifuged at 16,000 g for at least 30 minutes before loading into capillary tubes to remove all potential nucleation sites for freezing from the aqueous solutions. 2-3 mM F_nY-GB1 was measured from -15 ℃ to 80 ℃ in 100% (v/v) D_2O. 7.3 mM 2,6-F_2Y-UBQ was measured from -8 ℃ to 60 ℃ in 20 mM HEPES, 150 mM NaCl, pH 7.5, with 100% (v/v) D_2O. 2.2 mM 2,6-F_2Y-HPr was measured from -10 ℃ to 75 ℃, and 0.6 mM Y64F variant from 0 ℃ to 70 ℃ in the same buffer as 2,6-F_2Y-UBQ. Other mutant samples for signal assignment were dissolved to 0.3 mM in 20 mM MES, 100 mM KCl, pH 6.5 for GB1, and 20 mM Tris, 150 mM NaCl, pH 7.5 for HPr, with 10% (v/v) D_2O, using a regular 5 mm NMR tube.

For in-cell NMR, the samples of *E. coli* cells were prepared by inducible expression as described,[51] producing approximately 0.4 mM 2,6-F_2Y-HPr-Y64F in cells for experiments. The samples of A2780 cells were prepared as described,[52] and 5 mM 2,6-F_2Y-HPr-Y64F was used for electroporation to produce approximately 0.2 mM protein in cells (about 5.2×10^7 cells) for experiments. The samples of *X. laevis* oocytes were prepared as described[53], and 10 mM 2,6-F_2Y-HPr-Y64F was used for microinjection to produce approximately 0.3 mM protein in oocytes for experiments. The samples of mimicking the macromolecule crowded environment were prepared by dissolving 300 mg/mL Ficoll 70K in 20 mM HEPES buffer containing 150 mM NaCl, pH 7.5, with 10% (v/v) D_2O.

NMR spectra were recorded on Bruker Avance Spectrometers at 500 MHz with a double-resonance broadband probe or at 600, 700 and 850 MHz with a triple-resonance cryogenic probe. ^{19}F NMR temperature-variable experiments, covering the range from -15 ℃ to 80 ℃, were recorded at 500 MHz, with 256-512 scans, the chemical shifts were calibrated by internal reference of trifluorotoluene (-63.72 ppm at 25 ℃). Notably, capillary samples must be slowly cooled (reduce 1 ℃ every 3 minutes) in order to realize temperatures well below 0 ℃ and to maintain supercooled state without freezing. ^{19}F NMR assignment experiments, in-cell experiments were recorded at 600 MHz with 256 scans. ^{1}H-^{15}N HSQC spectra were recorded at 600 or 700 MHz at 25 ℃ with 8 scans, 2 s relaxation delay and 2048 and 128 complex points in the direct and indirect dimensions, respectively. ^{1}H-^{15}N SOFAST HMQC spectra for living cell samples were recorded at 850 MHz at 25 ℃ with 128-512 scans, 2048 and 256 complex points in the direct and indirect dimensions, respectively.

MS Measurement

Mass spectra were recorded on Agilent Technologies 6530 (Q-TOF) with an ESI source and connected to Agilent HPLC 1200 series equipped with an Agilent ZORBAX SB-C3, 5μm, 4.6×150 mm HPLC column. About 20 μM sample was injected using a l mL/min linear gradient of solvent A (0.1% (v/v) formic acid in water) and solvent B (acetonitrile), ramping solvent B from 5% at the start to 40% after 15 min, and the ESI source was in positive ion mode. Data were processed with Agilent Masshunter Qualitative Analysis.

Data Analysis

The NMR data were processed with Topspin 3.6.5. ^{19}F lineshape analysis was performed using the average density matrix theory with the DNMR module of TopSpin for two-state chemical exchange. The ^{19}F NMR spectra were used to obtain simulated lineshapes and the exchange rate, k_{ex}, based on initial parameters including the chemical shifts of the A and B states, signal intensity, line broadening, and fixed populations, $p_1 = p_2 = 0.5$. Activation parameters of the ring flip transition state were determined by non-linear regression of the ring flip rates, $k_{flip} = k_{ex}/2$, at the temperature T, using the Eyring equation,[25, 28, 54] i.e.,

$$k_{\text{flip}} = (\frac{k_{\text{B}}T}{h}) \times \exp[-(\Delta H^{\ddagger} - T\Delta S^{\ddagger})/RT] \qquad \text{eq 2}$$

where k_B, h, and R are Boltzmann's constant, Planck's constant, and the universal gas constant, respectively. T is the absolute temperature in Kelvin. $\Delta H^{\ddagger}$ and $\Delta S^{\ddagger}$ are the activation enthalpy and activation entropy, respectively, and they were assumed to be independent of T.

RESULTS

^{19}F spectra of tyrosine-fluorinated GB1

In order to find the sensitive ^{19}F probe for tyrosine ring flip dynamics, we synthesized a series of one- or two-fluorine-substituted tyrosines including 2FY, 3FY, 2,3-F_2Y, 2,6-F_2Y, 2,5-F_2Y and 3,5-F_2Y, via biological enzyme catalysis methods as previously described (Figure S1).[46] The synthesized fluorine-containing tyrosines were identified by ESI-MS and ^{19}F NMR, and the results were consistent with previous reports.[55-56] The fluorine-substituted tyrosines were each incorporated into the GB1 protein by natural biosynthesis in *E. coli*. The incorporation yields were determined by mass spectrometry (MS). GB1 contains three tyrosines Y3, Y45 and Y33. MS results show that the yields of GB1 with fluorine substitution at all three sites are 63.8% for 2FY-GB1, 53.2% for 2,6-F2Y-GB1, 73.4% for 2,3-F2Y-GB1,

62.9% for 3FY-GB1, 63.0% for 3,5-F2Y-GB1 and 61.7% for 2,5-F2Y-GB1, respectively. (Figure S2), indicating a good incorporation efficiency. We also assessed the effect of fluorine labelling on the GB1 structure by ^{1}H-^{15}N HSQC spectra (Figure S3). The signals of fluorinated GB1 proteins almost overlap with those of the wild type, suggesting that the effect of fluorination on GB1 structure is minimal. In this context, the 1D ^{19}F spectra of fluorinated GB1 were acquired, and assigned by site-specific mutation or according to our previous report (Figure 1 and S4-5).[57] Due to incomplete fluorine incorporation and high sensitivity of ^{19}F to fluorine or non-fluorine labelling states of surrounding aromatic residues, multiple ^{19}F signal peaks corresponding to one residue can be observed for some sites in ^{19}F spectra. The signals with high intensity were unambiguously assigned in ^{19}F spectra.

We analyzed ^{19}F spectra of fluorinated GB1 (Figure 1C-H). Firstly, the ^{19}F chemical shift distributions in GB1 are consistent with the corresponding free fluorinated tyrosines (Figure S6), suggesting that the chemical shifts mainly depend on the ^{19}F substituted position on the aromatic ring. Second, regardless of the ^{19}F substitution at the ε or δ site of the tyrosine, Y33 always exhibits a sharp peak, indicating that the aromatic rings of Y33 undergo fast exchange on the NMR time scale. Different from Y33, Y3 exhibits sharp (2,6-F_2Y-GB1 and 2,5-F_2Y-GB1), or severely broadened (2FY-GB1) or even disappeared (2,3-F_2Y-GB1) peaks, respectively, upon ^{19}F substitution at the δ site of tyrosine, suggesting that Y3 may undergo fast or intermediate exchange depending on the type of fluorinated tyrosines. In comparison, Y3 mainly exhibits fast exchange when ^{19}F is substituted at the ε site of tyrosine (3FY-GB1, 2,3-F_2Y-GB1, 3,5-F_2Y-GB1 and 2,5-F_2Y-GB1). Y45 with ^{19}F substitution at the ε site shows fast exchange properties like Y3. However, Y45 with ^{19}F substitution at the δ site shows intermediate exchange, yielding severely broadened or disappeared signals. Additionally, it is very interesting that for 2,3-F_2Y-GB1, the ^{19}F at the δ sites of both Y3 and Y45 do not give rise to similar peak shape to ε sites although they undergo the same ring flip process. The possible reason is that the two fluorine atoms at the δ and ε sites have different chemical shift anisotropy (CSA). Taken together, the above ^{19}F spectra of fluorinated GB1 suggest that Y3 and Y45 signals are more sensitive to the type of fluorinated tyrosines compared to Y33. This is probably due to the fact that Y33 is exposed on the surface and not involved in any particular stabilizing interactions, whereas Y3 and Y45 are close to hydrophobic core and interact by stacking with the π-cloud of the surrounding aromatic rings (Figure 1B).

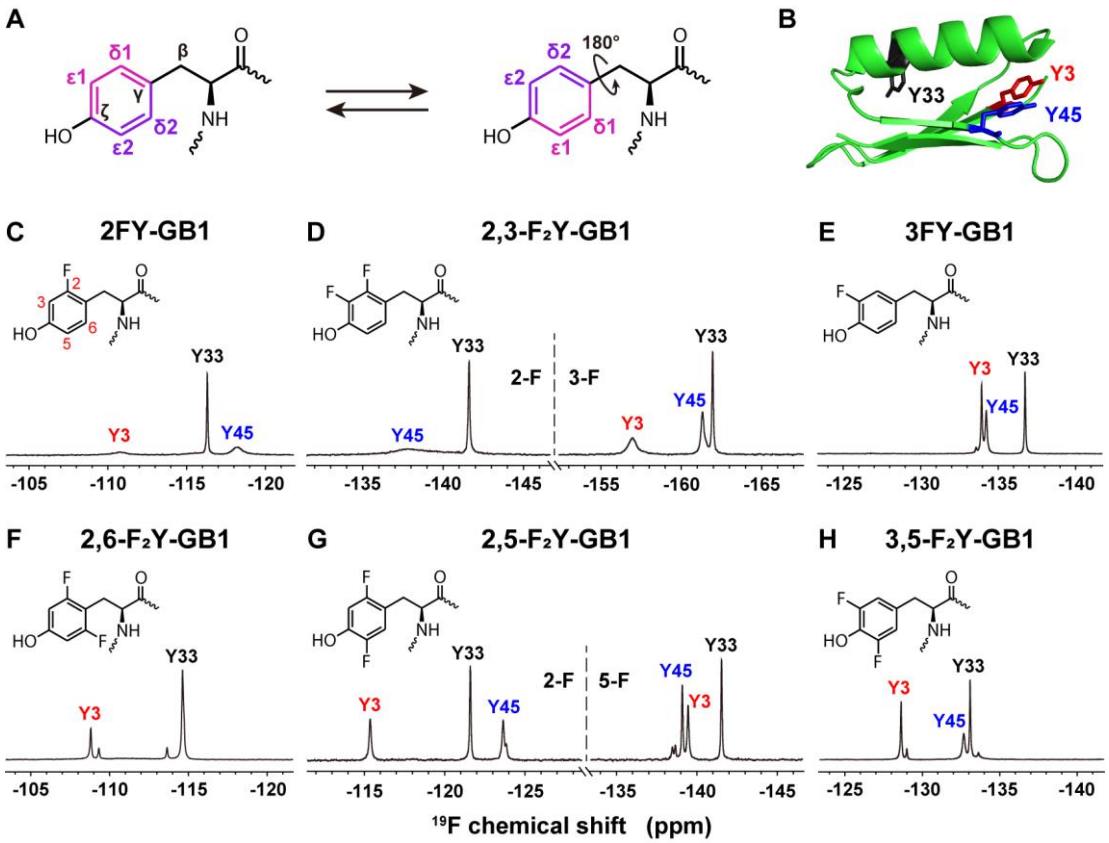

Figure 1. ^{19}F spectra of fluoroinated GB1. (A) Schematic illustration of a tyrosine residue undergoing 180° ring flips around the C_β-C_γ-C_ζ axis. (B) Cartoon representation of GB1 (PDB: 2J53). The side chains of Y3, Y45 and Y33 are shown as stick models, colored red, blue and black, respectively. (C)-(H) ^{19}F spectra of 2FY-GB1, 2,3-F_2Y-GB1, 3FY-GB1, 2,6-F_2Y-GB1, 2,5-F_2Y-GB1 and 3,5-F_2Y-GB1, respectively, at 25 °C. The inserts show the corresponding structure of fluorinated tyrosines.

Considering the temperature dependence of ring flips, we then acquired the variable-temperature ^{19}F spectra of fluorinated GB1 to observe the dynamic process of ring flips (the temperature ranges from -15 to 80 °C). As shown in Figure 2 and S7, 2,3-F_2Y-GB1 yields complex ^{19}F signals for Y3 and Y45 below 0 °C (Figure S7D), maybe because the coexistence of the slow ring flips around the C_β-C_γ-C_ζ axis and the torsion of the χ_1 dihedral angle around the C_α-C_β axis, which makes it difficult to analyze. For 3FY-GB1 and 2,5-F_2Y-GB1, none of the ^{19}F signals of the three Tyr residues exhibit a slow-to-fast ring flip process (Figure S7B and S7E). For 2FY-GB1, only a slow-to-fast ring flip process was observed for Y3, and for 3,5-F_2Y-GB1 only for Y45 (the signals are very weak) (Figure S7A and S7C). However, for 2,6-F_2Y-GB1, the slow-to-fast flip process was observed for Y45, the slow-to-intermediate process for Y3, and the intermediate-fast process for Y33 (Figure 2). These variable-temperature data suggest that 2,6-F_2Y is more sensitive to the ring flip process than the other fluorinated tyrosines. Therefore, based

on 2,6-F_2Y-GB1, we fitted the exchange rates (k_{ex}) of Y3 and Y45 by ^{19}F lineshape analysis (Table 1). From -15 to 80 ℃, Y45 undergoes a slow-to-fast process with k_{ex} from 233 to 7.1 $\times 10^5$ s^{-1} and Y3 undergoes a slow-to-intermediate process with k_{ex} from 6 to 6.0 $\times 10^3$ s^{-1}.

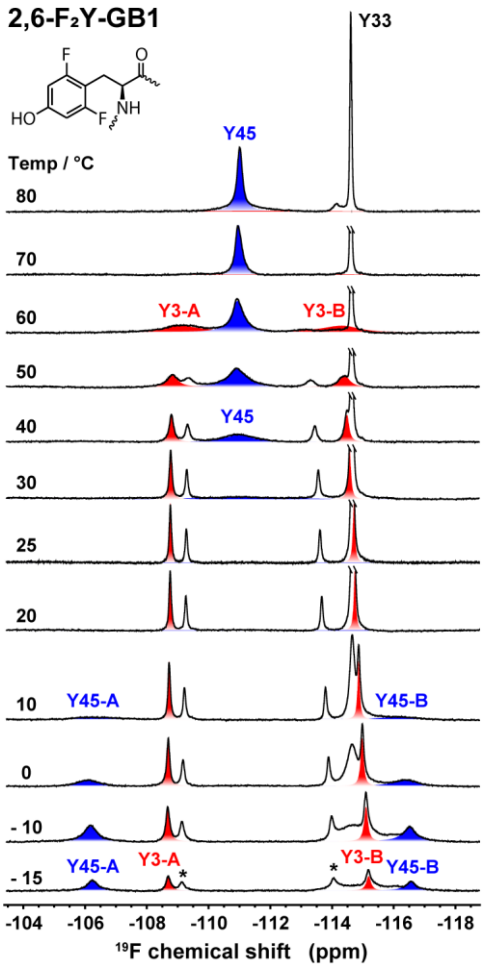

Figure 2. Ring flip dynamics of Y3 and Y45 in 2,6-F_2Y-GB1 at temperatures ranging from -15 ℃ to 80 ℃. The ^{19}F NMR spectra of 2,6-F_2Y-GB1 is shown in black curve, and the ^{19}F lineshape analysis spectra are shown in red and blue areas for Y3 and Y45, respectively. The inserts show the structure of 2,6-F_2Y. The asterisks indicate signals from Y3 due to incomplete fluorine incorporation. The signal intensity decreases at -15 ℃ compared to at -10 ℃, because partial protein samples in glass capillary tubes were frozen and thus can not yield signals.

Characterization of tyrosine ring flips of UBQ and HPr using 2,6-F_2Y

To validate the universal applicability of the 2,6-F_2Y probe, we further explored the ring flip dynamics of tyrosine residues in UBQ and HPr using 2,6-F_2Y labelling. Similar to GB1, the effect of fluorine substitution on the protein structures is small for UBQ and HPr (Figure S8-11). UBQ has only one tyrosine residue, Y59, which is largely buried (Figure 3A). The ^{19}F spectra of 2,6-F_2Y-UBQ show a

slow-to-fast exchange process from determined -8 ℃ to 25 ℃ (Figure 3B). Two isolated slowly-exchanged peaks (Y59-A and Y59-B) appear at T ≤ -5 ℃, and gradually exchange fast as the increasing temperature. The results of ^{19}F lineshape analysis show that they have a similar order of magnitude to the Y45 in 2,6-F_2Y-GB1 at the same temperature (Table 1). HPr contains three tyrosine residues, two of which (Y6 and Y37) are largely buried, and Y64 is exposed on the surface (Figure 3A). Based on the ^{19}F signal assignment (Figure S12), we found that Y6 in 2,6-F_2Y-HPr exhibits a slow-to-fast exchange process within the varied temperature range, and the two slow-exchanged separate peaks (Y6-A and Y6-B) can be observed with a ratio of 1:1 at ambient temperature. But ^{19}F signal of Y6-A severely overlaps with Y64. Therefore, we designed the Y64F variant, which shows the consistent dynamic changes with the wild type, to determine the subsequent ring flip rates (Figure 3C, S9B and S11B, and Table 1). The results of ^{19}F lineshape analysis indicate that Y6 undergoes a slow-to-fast process with k_{ex} of 2 to 1 $\times 10^4$ s^{-1} in the temperature range of 0 to 55 ℃.

The above studies of UBQ and HPr again show that 2,6-F_2Y is a sensitive probe for detecting ring flip dynamics, and it can provide the ring flip dynamics information on the time scale of microseconds to seconds under mild experimental conditions. Moreover, for the HPr protein system, which 2,6-F_2Y labelling shows a slow-to-fast exchange process at ambient temperature, it can be applied to quantify its ring flip rates in living cells by ^{19}F lineshape analysis due to the absence of background interference from cellular biological molecules.

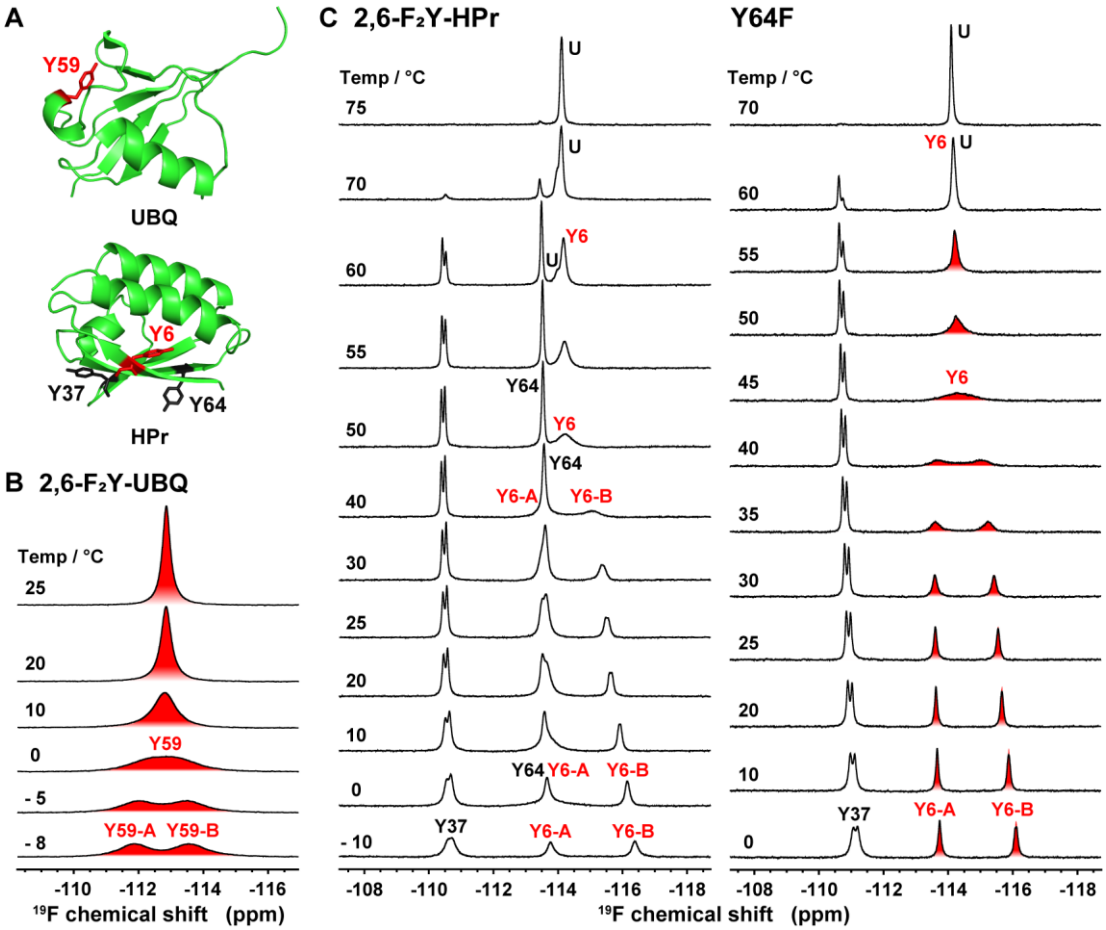

Figure 3. The ring flip dynamics of Y59 in 2,6-F_2Y-UBQ and Y6 in 2,6-F_2Y-HPr. (A) Cartoon representation of UBQ (PDB: 2LD9) and HPr (PDB: 1QR5). The side chains of Tyr are shown as stick models: Y59 of UBQ and Y6 of HPr are colored red, while Y37 and Y64 of HPr are colored black. (B) ^{19}F spectra of 2,6-F_2Y-UBQ at temperatures ranging from -8 °C to 25 °C. The red areas are ^{19}F lineshape analysis spectra of Y59. (C) ^{19}F spectra of 2,6-F_2Y-HPr at temperatures ranging from -10 °C to 75 °C, and of the Y64F variant at temperatures ranging from 0 °C to 70 °C. ^{19}F lineshape analysis spectra are shown in red areas. Due to incomplete fluorine incorporation and high sensitivity of ^{19}F to fluorine or non-fluorine labelling states of surrounding aromatic residues, Y37 exhibits two peaks (Figure S13).

Table 1. Exchange rates of aromatic ring flips in proteins obtained through 2,6-F_2Y labelling.

T / ℃	k_{ex} (k_{ex} = 2 k_{flip}) / s^{-1}							
	GB1		UBQ	HPr-Y64F				
					Y6 [e]			
	Y45 [a]	Y3 [b]	Y59 [c]	Y6 [d]	*E.coli*	A2780	Oocyte	Ficoll
80	7.1×10^5	6.0×10^3		unfold				
75				unfold				
70	4.2×10^5	2.4×10^3		unfold				
60	1.9×10^5	1.8×10^3	2.4×10^5	Partial unfold				
55				1.0×10^4				
50	1.0×10^5	531	1.1×10^5	4.9×10^3				
45				2.3×10^3				
40	5.1×10^4	184	5.8×10^4	767	1186	1005	869	516
37				452	951	722	526	294
35				296	816	588	352	162
30	1.6×10^4	94	2.2×10^4	106	539	350	141	62
25	9.1×10^3	60	1.6×10^4	38	332	188	59	23
20	5.0×10^3	53	1.1×10^4	3	269	98	4	3
10	2.4×10^3	43	3.9×10^3	3	215	83	4	2
0	1.0×10^3	30	1.2×10^3	2				
-5			641					
-8			434					
-10	477	16						
-15	233	6						

$\Delta\omega$: chemical shift difference between individual signals of both sides of the ring, [a]$\Delta\omega \approx 4800$ Hz and [b]$\Delta\omega \approx 3000$ Hz, from ^{19}F spectrum of 2,6-F_2Y-GB1 at 500 MHz and -15 ℃. [c]$\Delta\omega \approx 800$ Hz, from ^{19}F spectrum of 2,6-F_2Y-UBQ at 500 MHz and -8 ℃. [d]$\Delta\omega \approx 1100$ Hz, from ^{19}F spectrum of 2,6-F_2Y-HPr-Y64F at 500 MHz and 0 ℃. [e]$\Delta\omega \approx 1270$ Hz, from ^{19}F spectrum of 2,6-F_2Y-HPr-Y64F at 600 MHz and 10 ℃.

Tyrosine ring flip rate becomes faster in living cells

The ring flips of Y6 in 2,6-F_2Y-HPr-Y64F showed two slow exchange peaks at ambient temperature, which allows the ring flip dynamics to be investigated in living cells. Therefore, we introduced 2,6-F_2Y-HPr-Y64F into *E. coli* cells by over-expression, into A2780 cells by electroporation and into *X. laevis* oocytes by microinjection, respectively, and investigated its ring flip dynamics in cells. High-quality ^{19}F in-cell NMR spectra were acquired within the temperature range from 10 ℃ to 40 ℃ (Figure 4) and no leakage was observed (Figure S14). ^{19}F lineshape analysis revealed that Y6 flips faster in cells than in dilute solution, and flips fastest in *E. coli* cells, followed by A2780 cells and *X. laevis* oocytes (Table 1, Figure 4D). The flip rates in *X. laevis* oocytes approach those in dilute solution at the same temperature.

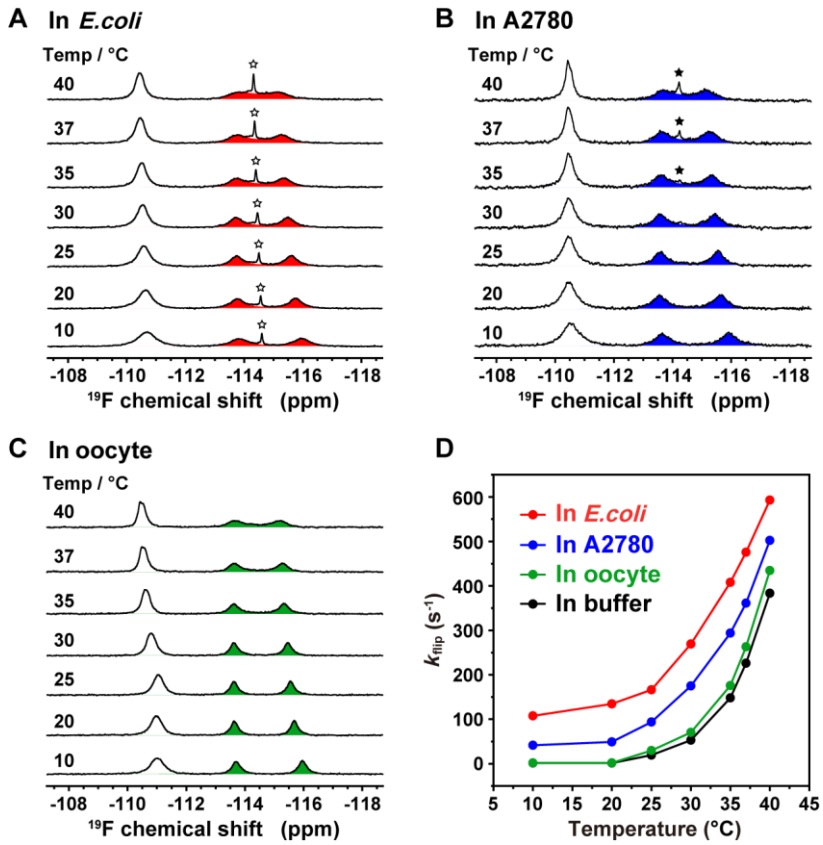

Figure 4. The ring flip dynamics of Y6 in 2,6-F_2Y-HPr-Y64F in living cells. (A)-(C) The ^{19}F spectra of 2,6-F_2Y-HPr-Y64F in *E. coli* cells, A2780 cells and *X. laevis* oocytes, respectively, at temperatures ranging from 10 °C to 40 °C. ^{19}F lineshape analysis spectra of Y6 are shown in red for *E. coli* cells, in blue for A2780 cells, and in green for *X. laevis* oocytes. The signals with (☆) labelled represent the free 2,6-F_2Y resonances, and the signals with (★) labelled represent the degradation resonances. (D) The ring flip rate (k_{flip}) of Y6 in *E. coli* cells (red), A2780 cells (blue), *X. laevis* oocytes (green) and diluted buffer (black) as a function of temperature.

The cellular environment is crowded and complex. In general, the macromolecular crowding effect and the quinary interactions between biological molecules have been considered to be two major factors affecting the structure, stability and dynamics of proteins.[30, 58-59] The size exclusion generated by macromolecular crowding generally causes proteins to form more compact conformations, which generally has a stabilizing effect for the protein. Theoretically, the crowding effect can decrease the flip rate because size exclusion results in limited space available for the targeted protein. We measured the ring flip rates of 2,6-F_2Y-HPr-Y64F in macromolecular crowding environments mimicked by the inert polymer Ficoll 70K (Table 1 and Figure S15). As expected, the reduced ring flip rates were observed compared to those in dilute solution. This suggests that macromolecular crowding is not the reason for the faster ring flip rates in cells.

Compared to the stabilizing effect of macromolecular crowding, the ubiquitous quinary interactions,

which have mainly a destabilizing effect, play a dominant role in affecting the protein stability in cells, as have been confirmed by in-cell stability studies of the proteins tested, including SH3, SOD1, GB1, and UBQ.[30] Moreover, the quinary interactions are also the main reason why NMR signals of proteins are severely broadened and even disappear inside cells.[47, 60-62] HPr is an acidic protein with pI 4.3. Theoretically, it can interact with biological molecules in relatively neutral cellular environment through hydrophobic and electrostatic interactions. As expected, the acquired in-cell ^{1}H-^{15}N HSQC spectra of 2,6-F_2Y-HPr-Y64F show that only background signals appear in *E. coli* cells, like ubiquitin protein.[47] The signals are visible, but obviously broadened in A2780 cells, followed by *X. laevis* oocytes (Figure S16). These observations confirm the strong interactions between HPr and biological molecules. The interactions are therefore thought to be responsible for the faster flip rates in the cells.

Activation parameters of aromatic ring flips from temperature-dependent analyses

In order to determine the kinetic activation parameters of the ring flips, i.e., the activation enthalpy ($\Delta H^{\ddagger}$) and the activation entropy ($\Delta S^{\ddagger}$), we analyzed the ring flip rates as a function of temperature using the Eyring equation (eq 2),[54] covering the range from -15 ℃ to 80 ℃ for GB1, from -8 ℃ to 60 ℃ for UBQ and from 25 ℃ to 60 ℃ for HPr for buffer samples, as well as from 25 ℃ to 40 ℃ for in-cell samples. Figure 5A shows k_{flip} plotted logarithmically as a function of 1/T for GB1-Y3 and -Y45, UBQ-Y59 and HPr-Y6. The plots are linear within the experimental error. The fitted $\Delta H^{\ddagger}$ and $\Delta S^{\ddagger}$ are in the same range as those reported for other proteins, which range from 50 to 150 kJ mol^{-1} for $\Delta H^{\ddagger}$ and 5 to 300 kJ mol^{-1} K^{-1} for $\Delta S^{\ddagger}$ (Table 2).[18] The $\Delta H^{\ddagger}$ represents the energy required for the ring to flip from the ground state to the transition state. Y3 and Y45 of GB1 and Y59 of UBQ have similar $\Delta H^{\ddagger}$ values in the buffer. However, Y6 of HPr has a large $\Delta H^{\ddagger}$ value of 150.8 ± 2.6 kJ mol^{-1}, although it is not completely buried in the hydrophobic core. Analysis of the HPr structure shows thatY6 interacts with the surrounding I61, T78 and L81 through hydrophobic interactions and (Figure 3A, S17), more importantly, the orientation of the aromatic ring of Y6 is almost parallel to the rigid β-sheet backbone on which it resides. We speculate that the increased hydrophobic interaction and the large steric hindrance effect resulting from the fluorine substitution, are likely to make the aromatic ring difficult to flip, and thus are responsible for large $\Delta H^{\ddagger}$.

Additionally, compared to the dilute solution, HPr-Y6 exhibits significantly reduced $\Delta H^{\ddagger}$ values in living cells, approximately a 58% reduction in *E. coli* cells, a 44% reduction in A2780 cells and a 9% reduction in *X. laevis* oocytes (Figure 5B and Table 2). This demonstrates an important influence of the

cellular environment on the dynamic process of ring flips. The cellular environment can remarkably increase the ability of ring flips by reducing the activation enthalpy, and the degree of increase depends on the cell type. The stronger the interaction, the more favorable it is for fast ring flipping. This implies that the cellular environment may regulate protein function by influencing aromatic ring flipping.

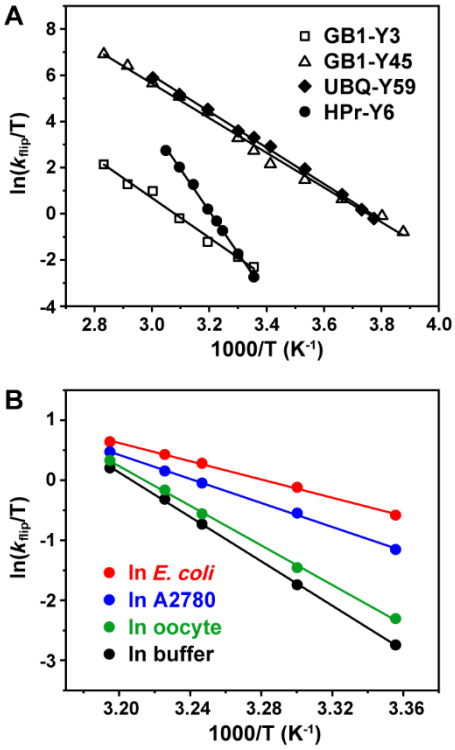

Figure 5. Temperature dependence of ring flip rates. ln(k_{flip}/T) is plotted as a function of 1/T. (A) The fitting lines of GB1-Y3 (square), GB1-Y45 (triangle), UBQ-Y59 (solid diamond) and HPr-Y6 (solid circle) in diluted buffer, respectively. (B) The fitting lines of HPr-Y6 in *E. coli* cells (red), A2780 cells (blue), *X. laevis* oocytes (green), and diluted buffer (black), respectively.

Table 2. Activation parameters of aromatic ring flips obtained by the Eyring equation.

Residue	Surroundings	$\Delta H^{\ddagger}$ (kJ mol^{-1})	$\Delta S^{\ddagger}$ (J mol^{-1} K^{-1})
GB1 - Y3	Buffer [a]	71.7 ± 3.4	23.3 ± 10.4
GB1 - Y45	buffer [a]	62.5 ± 1.6	36.8 ± 5.2
UBQ - Y59	buffer [a]	65.1 ± 1.1	47.7 ± 3.4
HPr - Y6	buffer [a]	150.8 ± 2.6	285.9 ± 8.0
HPr - Y6	*E. coli* [b]	63.2 ± 1.6	9.9 ± 5.1
HPr - Y6	A2780 [b]	83.2 ± 1.5	72.2 ± 4.8
HPr - Y6	Oocyte [b]	137.1 ± 2.2	243.1 ± 7.3

[a] Data from ^{19}F spectra acquired at 500 MHz. [b] Data from ^{19}F spectra acquired at 600 MHz.

DISCUSSION

According to previous studies, the two separate peaks in the slow exchange regime for the two symmetry-related nuclei of the aromatic ring arise under extreme conditions such as high pressure and/or low temperature. For example, Y3 of GB1 showed two split signals at -5 ℃ and 200 MPa,[13] while Y6 of HPr showed two split signals at 2 ℃ and 150-200 MPa.[10] Here, the two separate peaks in the slow exchange regime can be seen at normal temperature and pressure by introducing 2,6-F_2Y to increase the chemical shift difference of the δ-sites of Y3 in GB1 from 0.4 ppm (from reference 13) for $\Delta\omega_H$ to 6.5 ppm for $\Delta\omega_F$, and Y6 of HPr from 0.66 ppm (from reference 10) for $\Delta\omega_H$ to 2.4 ppm for $\Delta\omega_F$. Additionally, under the normal pressure condition, the two separate peaks in the slow exchange regime for Y45 of GB1 and Y59 of UBQ were also observed, which is challenging in the previous study due to fast flip.[18] The findings imply that, in the appearance of the NMR spectrum, the ring flip process, which is faster for the ^{1}H nucleus, becomes slower for the ^{19}F nucleus.

Additionally, we found that the 2,6-F_2Y substitution slowed down flip rates to varying degrees. For instance, the k_{flip} for Y45 of GB1 was found to be slightly slower than previously reported, while the k_{flip} for Y3 of GB1 was found to be 2 orders of magnitude slower.[13] The enhanced hydrophobic interaction of fluorocarbons compared to hydrocarbons was speculated to be the primary cause. It's also likely that the fluorine substitution increases the steric hindrance, making ring flips more difficult. Although fluorine-substituted aromatic rings likely introduce different interactions and dynamic properties than their native counterparts, it will hopefully improve the current situation where flip rates have only been measured for a limited number of proteins. Our statistical analysis of the chemical shifts of the δ- or ε-protons (H^δ and H^ε) of tyrosine aromatic ring in BioMagResBank shows that 1417 out of the 32618 (∽ 4.3%) tyrosine H^δ and H^ε pairs have different chemical shifts. This means that, based on the ^{1}H nucleus, only a very small fraction whose flip rates have the possibility to be determined under normal pressure. Our developed 2,6-F_2Y-substitution cause the ring flip process, which is faster for the ^{1}H nucleus, becomes slower for the ^{19}F nucleus in the appearance of the NMR spectrum. This will extend the range of detectable proteins. In addition, this ^{19}F NMR method is simple, convenient and inexpensive. There is no need for extreme conditions, complex signal assignments or expensive labelling compared to ^{1}H or ^{13}C-based methods. More importantly, due to the unique advantages of no background interference, it provides a powerful tool for measuring ring flip dynamics in complex environments such as living cells, which is always quite difficult to achieve. Using this method, we have for the first time successfully

characterized the ring flip dynamics of HPr-Y6 in three types of cells, and found that the cellular environments and cell types have a remarkable effect on ring flip dynamics.

CONCLUSION

In summary, we develop a convenient and efficient ^{19}F NMR method based on 2,6-F_2Y substitution to study the ring flip dynamics of tyrosine residues of proteins in dilute solution and complex biological environments. This method is used to characterize the tyrosine ring flip dynamics of three proteins GB1, UBQ and HPr, respectively, and shows a universal applicability on a wide time scales of microseconds to seconds. We also investigated the tyrosine ring flip dynamics of HPr within three types of living cells, including *E. coli* cells, A2780 cells, and *X. laevis* oocytes. For the first time, we found that tyrosine ring flip dynamics are remarkably affected by the cellular environment, and also depend on the cell type. The stronger the interactions, the lower the activation enthalpy, and the more favorable it is for fast ring flipping. Our study opens a window on protein ring flip events in biological environments.

ACKNOWLEDGMENTS

This work was supported by the National Natural Science Foundation of China [grants 21925406, 22374156, 21991082, 21921004], the Ministry of Science and Technology of China [grants 2021YFA1302600], and the Strategic Priority Research Program of the Chinese Academy of Sciences (XDB0540000 and YSBR-068).

REFERENCES

1. Lanzarotti, E.; Defelipe, L. A.; Marti, M. A.; Turjanski, A. G. Aromatic clusters in protein–protein and protein–drug complexes. *J. Cheminform.* **2020**, *12* (1), 30.
2. Yang, C.-J.; Takeda, M.; Terauchi, T.; Jee, J.; Kainosho, M. Differential large-amplitude breathing motions in the interface of FKBP12–drug complexes. *Biochemistry* **2015**, *54* (47), 6983-6995.
3. Ferreira, P.; Hernández-Ortega, A.; Lucas, F.; Carro, J.; Herguedas, B.; Borrelli, K. W.; Guallar, V.; Martínez, A. T.; Medina, M. Aromatic stacking interactions govern catalysis in aryl-alcohol oxidase. *FEBS J.* **2015**, *282* (16), 3091-3106.
4. Kumar, Y. B.; Kumar, N.; Vaikundamani, S.; Nagamani, S.; Mahanta, H. J.; Sastry, G. M.; Sastry, G. N. Analyzing the aromatic-aromatic interactions in proteins: A^2ID 2.0. *Int. J. Biol. Macromol.* **2023**, *253*, 127207.
5. Burley, S. K.; Petsko, G. A. Aromatic-aromatic interaction: a mechanism of protein structure stabilization. *Science* **1985**, *229* (4708), 23-28.
6. Brandl, M.; Weiss, M. S.; Jabs, A.; Sühnel, J.; Hilgenfeld, R. C-H···π-interactions in proteins. *J. Mol. Biol.* **2001**, *307* (1), 357-377.
7. Dougherty, D. A. Cation-pi interactions in chemistry and biology: a new view of benzene, phe, tyr, and trp. *Science* **1996**, *271* (5246), 163-168.

8. Wagner, G.; Wüthrich, K. Dynamic model of globular protein conformations based on NMR studies in solution. *Nature* **1978**, *275* (5677), 247-248.

9. Nall, B. T.; Zuniga, E. H. Rates and energetics of tyrosine ring flips in yeast iso-2-cytochrome c. *Biochemistry* **1990**, *29* (33), 7576-7584.

10. Hattori, M.; Li, H.; Yamada, H.; Akasaka, K.; Hengstenberg, W.; Gronwald, W.; Kalbitzer, H. R. Infrequent cavity-forming fluctuations in HPr from *Staphylococcus carnosus* revealed by pressure- and temperature-dependent tyrosine ring flips. *Protein Sci.* **2004**, *13* (12), 3104-3114.

11. Rao, D. K.; Bhuyan, A. K. Complexity of aromatic ring-flip motions in proteins: Y97 ring dynamics in cytochrome c observed by cross-relaxation suppressed exchange NMR spectroscopy. *J. Biomol. NMR* **2007**, *39* (3), 187-196.

12. Baturin, S. J.; Okon, M.; McIntosh, L. P. Structure, dynamics, and ionization equilibria of the tyrosine residues in *Bacillus circulans* xylanase. *J. Biomol. NMR* **2011**, *51* (3), 379-394.

13. Dreydoppel, M.; Raum, H. N.; Weininger, U. Slow ring flips in aromatic cluster of GB1 studied by aromatic ^{13}C relaxation dispersion methods. *J. Biomol. NMR* **2020**, *74* (2-3), 183-191.

14. Weininger, U.; Modig, K.; Akke, M. Ring flips revisited: ^{13}C relaxation dispersion measurements of aromatic side chain dynamics and activation barriers in basic pancreatic trypsin inhibitor. *Biochemistry* **2014**, *53* (28), 4519-4525.

15. Dreydoppel, M.; Akke, M.; Weininger, U. Characterizing fast conformational exchange of aromatic rings using residual dipolar couplings: distinguishing jumplike flips from other exchange mechanisms. *J. Phys. Chem. B* **2022**, *129* (40), 7950-7956.

16. Mariño Pérez, L.; Ielasi, F. S.; Bessa, L. M.; Maurin, D.; Kragelj, J.; Blackledge, M.; Salvi, N.; Bouvignies, G.; Palencia, A.; Jensen, M. R. Visualizing protein breathing motions associated with aromatic ring flipping. *Nature* **2022**, *602* (7898), 695-700.

17. Martin, B. T.; Malmstrom, R. D.; Amaro, R. E.; Wüthrich, K. OCRE domains of splicing factors RBM5 and RBM10: tyrosine ring-flip frequencies determined by integrated use of ^{1}H NMR spectroscopy and molecular dynamics simulations. *ChemBioChem* **2020**, *22* (3), 565-570.

18. Akke, M.; Weininger, U. NMR studies of aromatic ring flips to probe conformational fluctuations in proteins. *J. Phys. Chem. B* **2023**, *127* (3), 591-599.

19. Campbell, I. D.; Dobson, C. M.; Williams, R. J. Proton magnetic resonance studies of the tyrosine residues of hen lysozyme-assignment and detection of conformational mobility. *Proc. R. Soc. Lond. B. Biol. Sci.* **1975**, *189* (1097), 503-509.

20. Hull, W. E.; Sykes, B. D. Fluorotyrosine alkaline phosphatase: internal mobility of individual tyrosines and the role of chemical shift anisotropy as a ^{19}F nuclear spin relaxation mechanism in proteins. *J. Mol. Biol.* **1975**, *98* (1), 121-153.

21. Wagner, G.; Wüthrich, K. Proton NMR studies of the aromatic residues in the basic pancreatic trypsin inhibitor (BPTI). *J. Magn. Reson.* **1975**, *20* (3), 435-445.

22. Wüthrich, K.; Wagner, G. NMR investigations of the dynamics of the aromatic amino acid residues in the basic pancreatic trypsin inhibitor. *FEBS Lett.* **1975**, *50* (2), 265-268.

23. Campbell, I. D.; Dobson, C. M.; Moore, G. R.; Perkins, S. J.; Williams, R. J. P. Temperature dependent molecular motion of a tyrosine residue of ferrocytochrome C. *FEBS Lett.* **1976**, *70* (1), 96-100.

24. Li, H.; Yamada, H.; Akasaka, K. Effect of pressure on the tertiary structure and dynamics of folded basic pancreatic trypsin inhibitor. *Biophys. J.* **1999**, *77* (5), 2801-2812.

25. Skalicky, J. J.; Mills, J. L.; Sharma, S.; Szyperski, T. Aromatic ring-flipping in supercooled water:

implications for NMR-based structural biology of proteins. *J. Am. Chem. Soc.* **2001**, *123* (3), 388-397.
26. Weininger, U.; Respondek, M.; Löw, C.; Akke, M. Slow aromatic ring flips detected despite near-degenerate NMR frequencies of the exchanging nuclei. *J. Phys. Chem. B* **2013**, *117* (31), 9241-9247.
27. Weininger, U.; Brath, U.; Modig, K.; Teilum, K.; Akke, M. Off-resonance rotating-frame relaxation dispersion experiment for ^{13}C in aromatic side chains using L-optimized TROSY-selection. *J. Biomol. NMR* **2014**, *59* (1), 23-29.
28. Dreydoppel, M.; Dorn, B.; Modig, K.; Akke, M.; Weininger, U. Transition-state compressibility and activation volume of transient protein conformational fluctuations. *JACS Au* **2021**, *1* (6), 833-842.
29. Dreydoppel, M.; Lichtenecker, R. J.; Akke, M.; Weininger, U. ^{1}H $R_{1\rho}$ relaxation dispersion experiments in aromatic side chains. *J. Biomol. NMR* **2021**, *75* (10-12), 383-392.
30. Xu, G.; Cheng, K.; Liu, M.; Li, C. Studying protein stability in crowded environments by NMR. *Prog. Nucl. Magn. Reson. Spectrosc.* **2024**, *140*, 42-48.
31. Chai, Z.; Li, C. In-cell ^{19}F NMR of proteins: recent progress and future opportunities. *Chem. Eur. J.* **2024**, *30* (23), e202303988.
32. Chen, H.; Viel, S.; Ziarelli, F.; Peng, L. ^{19}F NMR: a valuable tool for studying biological events. *Chem Soc Rev* **2013**, *42* (20), 7971-82.
33. Boeszoermenyi, A.; Chhabra, S.; Dubey, A.; Radeva, D. L.; Burdzhiev, N. T.; Chanev, C. D.; Petrov, O. I.; Gelev, V. M.; Zhang, M.; Anklin, C.; Kovacs, H.; Wagner, G.; Kuprov, I.; Takeuchi, K.; Arthanari, H. Aromatic ^{19}F-^{13}C TROSY: a background-free approach to probe biomolecular structure, function, and dynamics. *Nat. Methods* **2019**, *16* (4), 333-340.
34. Rose-Sperling, D.; Tran, M. A.; Lauth, L. M.; Goretzki, B.; Hellmich, U. A. ^{19}F NMR as a versatile tool to study membrane protein structure and dynamics. *Biol. Chem.* **2019**, *400* (10), 1277-1288.
35. Boeszoermenyi, A.; Ogórek, B.; Jain, A.; Arthanari, H.; Wagner, G. The precious fluorine on the ring: fluorine NMR for biological systems. *J. Biomol. NMR* **2020**, *74* (8-9), 365-379.
36. Buchholz, C. R.; Pomerantz, W. C. K. ^{19}F NMR viewed through two different lenses: ligand-observed and protein-observed ^{19}F NMR applications for fragment-based drug discovery. *RSC Chem Biol* **2021**, *2* (5), 1312-1330.
37. Gimenez, D.; Phelan, A.; Murphy, C. D.; Cobb, S. L. ^{19}F NMR as a tool in chemical biology. *Beilstein J. Org. Chem.* **2021**, *17*, 293-318.
38. Orton, H. W.; Qianzhu, H.; Abdelkader, E. H.; Habel, E. I.; Tan, Y. J.; Frkic, R. L.; Jackson, C. J.; Huber, T.; Otting, G. Through-space scalar ^{19}F-^{19}F couplings between fluorinated noncanonical amino acids for the detection of specific contacts in proteins. *J. Am. Chem. Soc.* **2021**, *143* (46), 19587-19598.
39. Gronenborn, A. M. Small, but powerful and attractive: ^{19}F in biomolecular NMR. *Structure* **2022**, *30* (1), 6-14.
40. Zhu, W.; Guseman, A. J.; Bhinderwala, F.; Lu, M.; Su, X.-C.; Gronenborn, A. M. Visualizing proteins in mammalian cells by ^{19}F NMR spectroscopy. *Angew. Chem. Int. Ed.* **2022**, *61* (23), e202201097.
41. Huang, Y.; Reddy, K. D.; Bracken, C.; Qiu, B.; Zhan, W.; Eliezer, D.; Boudker, O. Environmentally ultrasensitive fluorine probe to resolve protein conformational ensembles by ^{19}F NMR and Cryo-EM. *J. Am. Chem. Soc.* **2023**, *145* (15), 8583-8592.
42. Pham, L. B. T.; Costantino, A.; Barbieri, L.; Calderone, V.; Luchinat, E.; Banci, L. Direct expression of fluorinated proteins in human cells for ^{19}F in-cell NMR spectroscopy. *J. Am. Chem. Soc.* **2023**, *145* (2), 1389-1399.
43. Qianzhu, H.; Abdelkader, E. H.; Otting, G.; Huber, T. Genetic encoding of fluoro-L-tryptophans for

site-specific detection of conformational heterogeneity in proteins by NMR spectroscopy. *J. Am. Chem. Soc.* **2024**, *146* (19), 13641-13650.

44. Sengupta, I. Insights into the structure and dynamics of proteins from ^{19}F solution NMR spectroscopy. *Biochemistry* **2024**, *63* (22), 2958-2968.

45. Xu, S.; Zhang, Y.; Li, Y.; Xia, X.; Zhou, J.; Shi, G. Production of L-tyrosine using tyrosine phenol-lyase by whole cell biotransformation approach. *Enzyme Microb. Technol.* **2019**, *131*, 109430.

46. Seyedsayamdost, M. R.; Yee, C. S.; Stubbe, J. Site-specific incorporation of fluorotyrosines into the R2 subunit of *E.coli* ribonucleotide reductase by expressed protein ligation. *Nat. Protoc.* **2007**, *2* (5), 1225-1235.

47. Xu, G.; Ye, Y.; Liu, X.; Cao, S.; Wu, Q.; Cheng, K.; Liu, M.; Pielak, G. J.; Li, C. Strategies for protein NMR in *Escherichia coli*. *Biochemistry* **2014**, *53* (12), 1971-1981.

48. Li, C.; Lutz, E. A.; Slade, K. M.; Ruf, R. A. S.; Wang, G.-F.; Pielak, G. J. ^{19}F NMR studies of α-synuclein conformation and fibrillation. *Biochemistry* **2009**, *48* (36), 8578-8584.

49. Kruse, R.; Hengstenberg, W.; Beneicke, W.; Kalbitzer, H. R. Involvement of various amino- and carboxyl-terminal residues in the active site of the histidine-containing protein HPr of the phosphoenolpyruvate-dependent phosphotransferase system of *Staphylococcus carnosus*: site-directed mutagenesis with the ptsH gene, biochemical characterization and NMR studies of the mutant proteins. *Protein Eng.* **1993**, *6* (4), 417-423.

50. Skalicky, J. J.; Sukumaran, D. K.; Mills, J. L.; Szyperski, T. Toward structural biology in supercooled water. *J. Am. Chem. Soc.* **2000**, *122* (13), 3230-3231.

51. Wu, Q.; Liu, X.; Chai, Z.; Cheng, K.; Xu, G.; Jiang, L.; Liu, M.; Li, C. Lanmodulin remains unfolded and fails to interact with lanthanide ions in *Escherichia coli* cells. *Chem. Commun.* **2022**, *58* (59), 8230-8233.

52. Chai, Z.; Wu, Q.; Cheng, K.; Liu, X.; Zhang, Z.; Jiang, L.; Zhou, X.; Liu, M.; Li, C. Visualizing proteins in human cells at near-physiological concentrations with sensitive ^{19}F NMR chemical tags. *Angew. Chem. Int. Ed.* **2023**, *62* (22), e202300318.

53. Ye, Y.; Liu, X.; Xu, G.; Liu, M.; Li, C. Direct observation of Ca^{2+}-induced calmodulin conformational transitions in intact *Xenopus laevis* oocytes by ^{19}F NMR spectroscopy. *Angew. Chem. Int. Ed.* **2015**, *54* (18), 5328-5330.

54. Eyring, H. The activated complex in chemical reactions. *J. Chem. Phys.* **1935**, *3* (2), 107-115.

55. Seyedsayamdost, M. R.; Reece, S. Y.; Nocera, D. G.; Stubbe, J. Mono-, di-, tri-, and tetra-substituted fluorotyrosines: new probes for enzymes that use tyrosyl radicals in catalysis. *J. Am. Chem. Soc.* **2006**, *128* (5), 1569-1579.

56. Kim, K.; Cole, P. A. Kinetic analysis of a protein tyrosine kinase reaction transition state in the forward and reverse directions. *J. Am. Chem. Soc.* **1998**, *120* (28), 6851-6858.

57. Ye, Y.; Liu, X.; Zhang, Z.; Wu, Q.; Jiang, B.; Jiang, L.; Zhang, X.; Liu, M.; Pielak, G. J.; Li, C. ^{19}F NMR spectroscopy as a probe of cytoplasmic viscosity and weak protein interactions in living cells. *Chem. Eur. J.* **2013**, *19* (38), 12705-12710.

58. Miklos, A. C.; Li, C.; Sharaf, N. G.; Pielak, G. J. Volume exclusion and soft interaction effects on protein stability under crowded conditions. *Biochemistry* **2010**, *49* (33), 6984-6991.

59. Smith, A. E.; Zhou, L. Z.; Gorensek, A. H.; Senske, M.; Pielak, G. J. In-cell thermodynamics and a new role for protein surfaces. *Proc. Natl. Acad. Sci. USA* **2016**, *113* (7), 1725-1730.

60. Speer, S. L.; Stewart, C. J.; Sapir, L.; Harries, D.; Pielak, G. J. Macromolecular crowding is more than hard-core repulsions. *Annu. Rev. Biophys.* **2022**, *51* (1), 267-300.

61. Li, C.; Charlton, L. M.; Lakkavaram, A.; Seagle, C.; Wang, G.; Young, G. B.; Macdonald, J. M.; Pielak, G. J. Differential dynamical effects of macromolecular crowding on an intrinsically disordered protein and a globular protein: implications for in-cell NMR spectroscopy. *J. Am. Chem. Soc.* **2008**, *130* (20), 6310-6311.
62. Smith, A. E.; Zhang, Z.; Pielak, G. J.; Li, C. NMR studies of protein folding and binding in cells and cell-like environments. *Curr. Opin. Struct. Biol.* **2015**, *30*, 7-16.